Int. J. Nano Dimens., 8 (2): 107-113, Spring 2017

ORIGINAL ARTICLE

A novel lightly doped drain and source Carbon nanotube field effect transistor (CNTFET) with negative differential resistance

Seyed Ali Sedigh Ziabari [1]; Mohammad Javad Tavakoli Saravani [2]*

[1]*Department of Electrical Engineering, Rasht Branch, Islamic Azad University, Rasht, Iran*
[2]*Department of Electrical Engineering, Mehrastan Institute of Higher Education, Astaneh Ashrafieh, Iran*

Received 27 December 2016; revised 18 February 2017; accepted 07 March 2017; available online 14 March 2017

Abstract

In this paper, we propose and evaluate a novel design of a lightly doped drain and source carbon nanotube field effect transistor (LDDS-CNTFET) with a negative differential resistance (NDR) characteristic, called negative differential resistance LDDS-CNTFET (NDR-LDDS-CNTFET). The device was simulated by using a non equilibrium Green's function method. To achieve this phenomenon, we have created two quantum wells in the intrinsic channel by using two n-type regions. In the wells that are separated by a thin barrier, two resonance states are generated. On the other hand, the thickness of the barrier between the source and the well is variable depending on the energy level. Accordingly, with increasing gate-source voltage, the number of tunneling electrons and consequently drain-source current are varied. Furthermore, we have presented a structure with two n-type and three p-type regions in the channel that illustrates a larger NDR region. In this structure, the peak and valley of the drain-source current are shifted when compared with the previous structure. Finally, we investigated the effect of doping concentration on the NDR parameter.

Keywords: *Carbon nanotube; Lightly doped drain and source (LDDS); Negative differential resistance; Resonance energy states; Quantum well.*

How to cite this article

Sedigh Ziabari S. A., Tavakoli Saravani M. J., A novel lightly doped drain and source Carbon nanotube field effect transistor (CNTFET) with negative differential resistance. Int. J. Nano Dimens., 2017; 8(2): 107-113., DOI: 10.22034/ijnd.2017.24833

INTRODUCTION

In the recent years, negative differential resistance (NDR) devices, particularly resonant tunneling diode (RTD), have attracted considerable attention [1-3]. Some of the NDR applications are in voltage- controlled oscillator (VCO) [1, 2], RTD terahertz oscillators [2, 3], logic circuits, high frequency, and memory devices [4]. For example, recently tunneling diodes have attracted much interest in the implementation of low power oscillators, due to the inherent NDR characteristics achieved at a lower applied voltage [1]. In addition to RTD, researchers have devoted a lot of attention to achieve other devices with NDR characteristics. For example, a nitrogen-passivated zigzag grapheme nano-ribbon field effect transistor structure has proposed that it shows an NDR phenomenon, which can be controlled by variation of the potential applied at the gate of the device [4]. A vertical tunneling field effect transistor using a stacked double bilayer graphene (BLG) and hexagonal boron nitride (HBN) heterostructure has presented, which shows two tunneling resonances with negative differential resistance [5]. The three-terminal λ-type NDR tunneling real-space transfer transistors (TRSTT) with InGaAs and a δ-doped GaAs dual-channel structure on a GaAs substrate has been demonstrated [6]. Structures with real-space transfer (RST) phenomena have been widely studied [7-9]. The negative differential resistance graphene nanoribbon superlattice field effect transistors (NDR-GNSL-FETs) have also been proposed [10]. As it can be observed, until the recent years, there is not much work in the field of NDR in the nano-transistors.

Previously, the structure of lightly doped drain and source CNTFET (LDDS-CNTFET) was proposed with a modification of the MOSCNT by utilizing lightly doped regions between the intrinsic channel and the highly doped source and drain regions. Numerical simulations illustrate that this device has superior characteristics when compared with MOSCNT and linearly doped CNTFET (LD-CNTFET) [11]. In this paper, we have proposed a novel

* Corresponding Author Email: *sedigh@iaurasht.ac.ir*

LDDS-CNTFET with negative differential resistance characteristic (NDR-LDDS-CNTFET) based on a special doping profile in the channel region.

EXPERIMENTAL

Device Structure and Computational Method

The 2D cross-sectional view of the proposed NDR-LDDS-CNTFET is illustrated in Fig. 1. The CNT is assumed (16, 0) with a radius of 0.63 nm. The gate dielectric layer is HfO_2 with thickness 2 nm and ε_r=16. The doping concentrations in the high source and drain regions and LDDS regions, which are defined as N_1 and N_2, are 2×10^9 m^{-1} and 0.2×10^9 m^{-1}, respectively. We have divided the channel into five regions (1-5) with lengths of 2.2, 4, 2.6, 4, and 2.2 nm, respectively. Each region is associated with a specific concentration, as will be shown Tables 1 and 2.

The device has been simulated by self consistent solution of the Poisson and Schrodinger equations. The electrostatic potential of CNT is calculated by solving the Poisson equation in cylindrical coordinates. The carrier concentrations are calculated by solving the Schrodinger equation within the NEGF formalism [11-14]. The retarded Green's function is calculated as [11-14]

$$G(E) = [EI - H - \Sigma_S - \Sigma_D]^{-1} \quad (1)$$

where E is the energy, I the identity matrix, H the Hamiltonian of the CNT and Σ_S and Σ_D the self-energies of the source and drain, respectively. We calculate transmission at each energy point E by [11-14],

$$T(E) = \mathrm{tr}\{\Gamma_S G \Gamma_D G^{\dagger}\} \quad (2)$$

where $\Gamma_S = i(\Sigma_S - \Sigma_S^{\dagger})$, and $\Gamma_S = i(\Sigma_D - \Sigma_D^{\dagger})$.

Finally, the current flow is given by

$$I = \frac{4e}{\hbar}\int_{-\infty}^{+\infty}\frac{dE}{2\pi}T(E)[f(E-E_{FS}) - f(E-E_{FD})] \quad (3)$$

where *f(E)* is the Fermi distribution, and E_{FS} and E_{FD} are source and drain Fermi energies, respectively. The simulation has been done by MATLAB. In order to illustrate the accuracy of our simulation, we have simulated an LDDS-CNTFET with intrinsic channel, which represented in [11]. Fig. 2 shows the simulated I_{DS}–V_{GS} characteristics of this transistor and compares it with the result in [11].

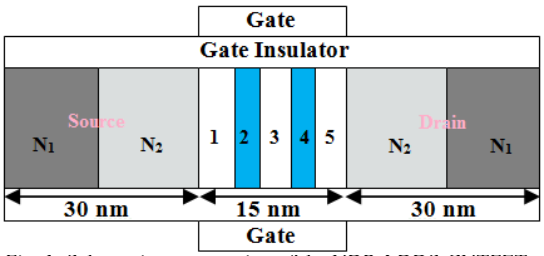

Fig. 1: Schematic cross-section of the NDR-LDDS-CNTFET.

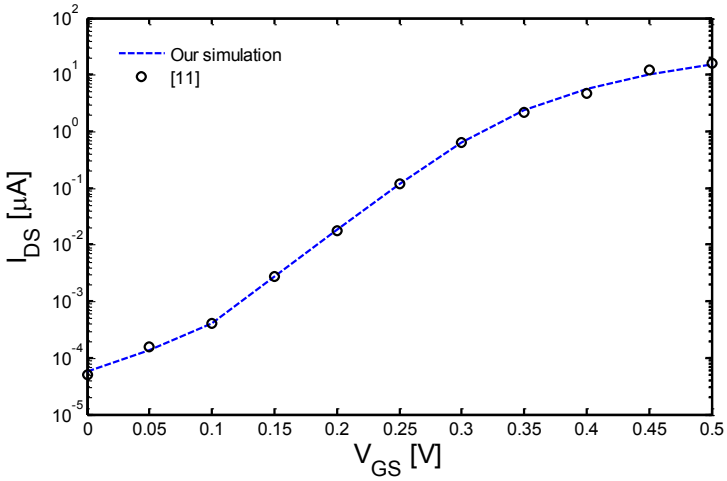

Fig. 2: The simulated IDS–VGS characteristics of the MOSCNT and compares it with the result in [11].

RESULTS AND DISCUSSIONS

At first, we assumed that the regions 1, 3, and 5 are intrinsic and the doping concentrations in regions 2 and 4 are defined according to Table 1. We calculated the I_{DS}-V_{GS} characteristics for different types of the NDR-LDDS-CNTFET, as shown in Table 1, with the voltage bias V_{DS}=0.4 V. These results are illustrated in Fig. 3. This figure shows that the I_{DS} decrease with increase in V_{GS} for a *distinct* region, which implies NDR. We *consider* the parameter of NDR to be defined as $\Delta V/\Delta I$, where $\Delta I=I_V-I_P$, $\Delta V= V_V-V_P$, in which I_P, I_V, V_P, and V_V are the peak of current, the valley of current, the peak of voltage, and the valley of voltage, respectively. In type 1 structure, for V_{GS} lower than 0.025 V, the drain-source current increases with increase in V_{GS}. As V_{GS} increases above 0.025 V, the I_{DS} monotonously decrease. The I_{DS} increases for the gate-source voltage more than 0.075 V. Thus, the proposed device exhibits the NDR characteristic over the range of V_{GS}= 0.025-0.075 V. This figure also demonstrates that with decreasing n-type doping concentrations of regions 2 and 4, the peak and valley have shifted and increased.

The energy band diagram and color-scaled plot for the number of electrons are simulated for type 1 with V_{GS} = -0.05 V and V_{DS} = 0.4 V, as shown in Fig. 4. This figure illustrates that the proposed channel doping profile creates the two potential wells in the conduction band that are separated by a thin potential barrier. Therefore, two resonance states are generated due to coupling between the ground-states of the left and right

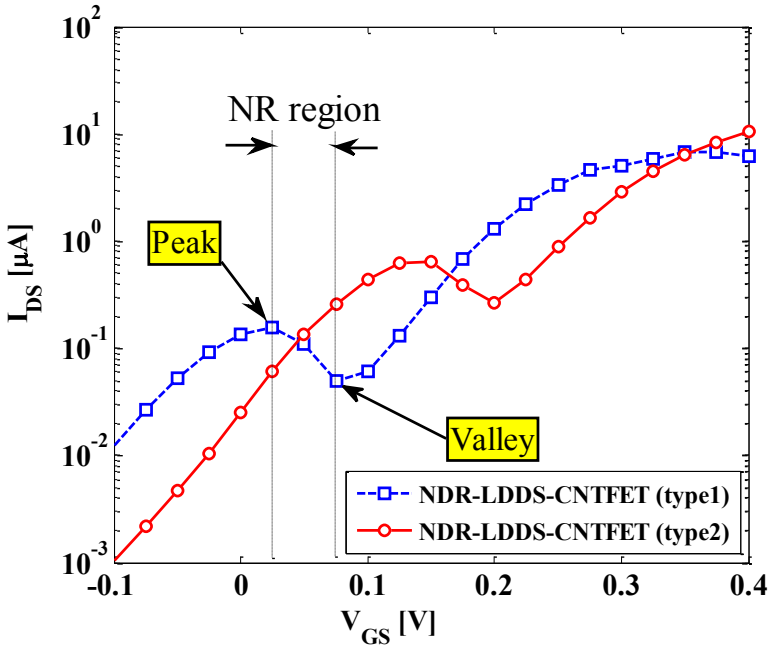

Fig. 3: The IDS-VGS characteristics of NDR-LDDS-CNTFET, calculated for various types of devices of Table I, at VDS=0.4 V. The NDR region has been marked for NDR-LDDS-CNTFET of type 1.

Table 1: Doping concentrations in regions 2 and 4 of the channel.

	n-type doping concentrations in regions 2 and 4
NDR-LDDS-CNTFET (type 1)	2×10^{9} m^{-1}
NDR-LDDS-CNTFET (type 2)	1.4×10^{9} m^{-1}

wells [15]. The lowest-energy resonance state at E_0 and upper-energy resonance state at E_1 are also demonstrated in Fig. 4.

To investigate the NDR phenomenon, the energy band diagram and color-scaled plot for the number of electrons for type 1 with V_{GS}= -0.05 V, 0.025 V, 0.05 V, and 0.075 V are shown in Fig. 5. With increase in the gate voltage, E_0 and E_1 decrease. As observed in this comparison, in Fig. 5(b), the states are increasingly filled by tunneling electrons in comparison with (a). Also, Fig. 4(c) and (d) show that with biases of V_{GS}=0.05 V and V_{GS}=0.075 V, despite the increase in V_{GS}, the number of tunneling electrons in the lowest-energy state decreases. The reason for this phenomenon is the increase in region 1 barrier thickness for the lowest-energy state. The I_{DS} increases for V_{GS} more than about 0.075 V due to the approach of the channel potential barrier to the source Fermi level.

Furthermore, we presented the NDR-LDDS-CNTFET structure with the p-type doping in the regions 1, 3, and 5 according to Table 2. We simulated the I_{DS}-V_{GS} characteristics of the structures of types 3 and 4 at a given V_{DS} of 0.4 V as shown in Fig. 6.

In this figure, the peak and valley of type 3 are shifted when compared with type 2 of Fig. 3. To explain these effects, we have calculated the energy band diagram and color-scaled plot for the number of electrons for types 2 and 3 at V_{DS}= 0.4 V and V_{GS}= 0.1 V, which are illustrated in Fig. 7. As seen in this figure, in type 3 structure that has deep wells; two resonance states E_0 and E_1 are higher in comparison with that for type 2. This figure also shows that type 4 structure with the doping concentrations in the regions 1, 3, and 5 is higher than that of type 3, showing the shift and the reduction of the peak and valley in comparison with that in type 3.

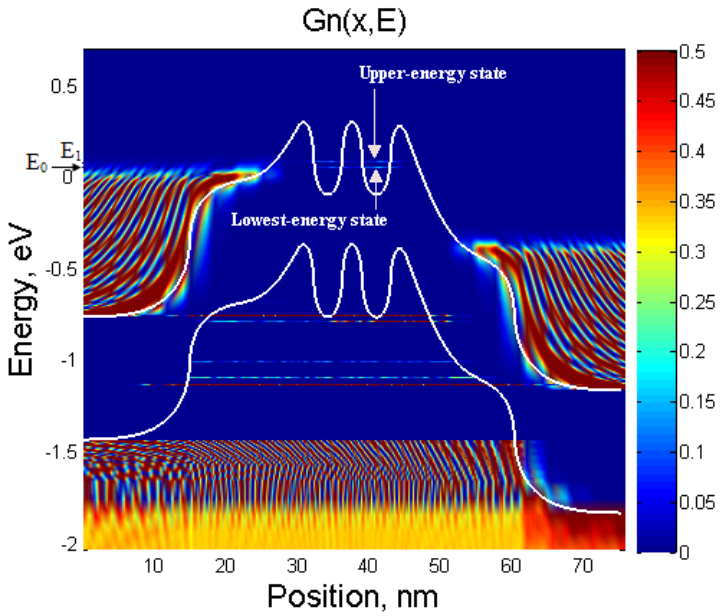

Fig. 4: The energy band diagram and color-scaled plot for the number of electrons per unit energy along the CNT axis for type 1 with VGS = -0.05 V and VDS = 0.4 V.

Table 2: Doping concentrations in regions 1-5 of channel.

	p-type doping concentration in regions 1, 3, and 5	n-type doping concentration in regions 2 and 4
NDR-LDDS-CNTFET (type 3)	0.9×10^{9} m^{-1}	1.4×10^{9} m^{-1}
NDR-LDDS-CNTFET (type 4)	1.3×10^{9} m^{-1}	1.4×10^{9} m^{-1}

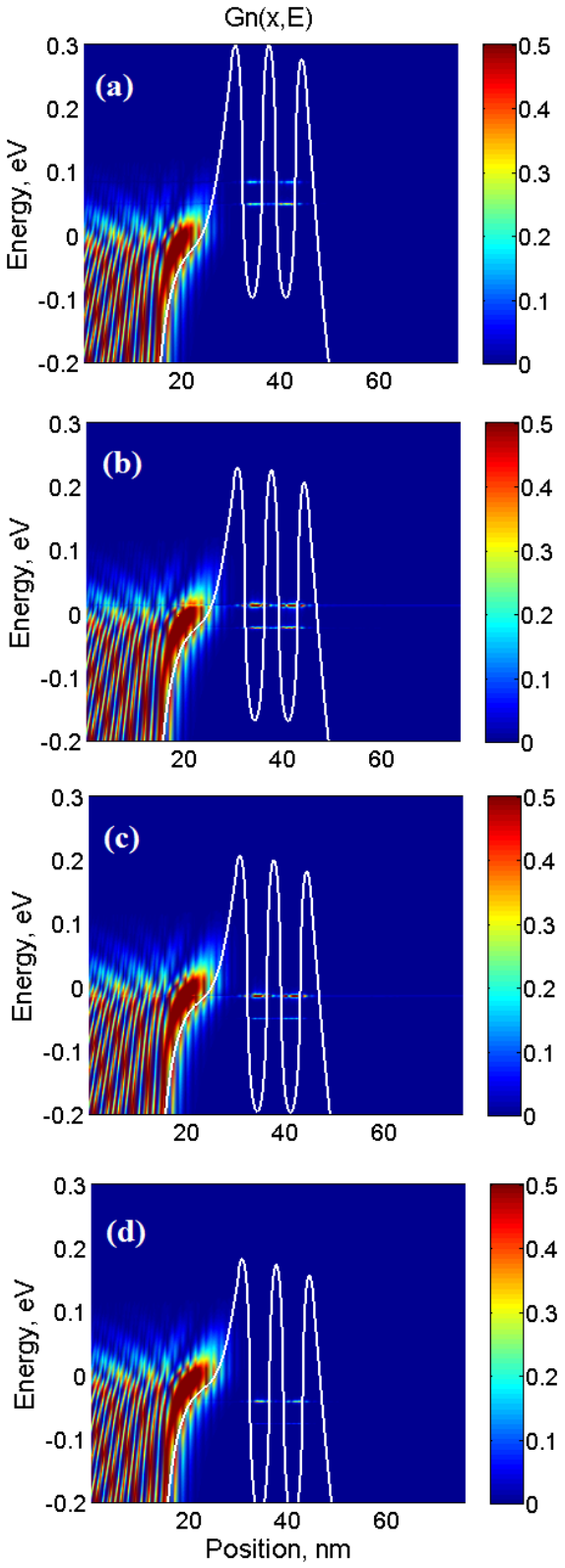

Fig. 5: The energy band diagram and color-scaled plot for the number of electrons per unit energy along the CNT axis for NDR-LDDS-CNTFET (type 1) at (a) VGS= -0.05 V, (b) VGS=0.025 V, (c) VGS=0.05 V, (d) VGS=0.075 V. The drain-source bias for all four cases is 0.4 V.

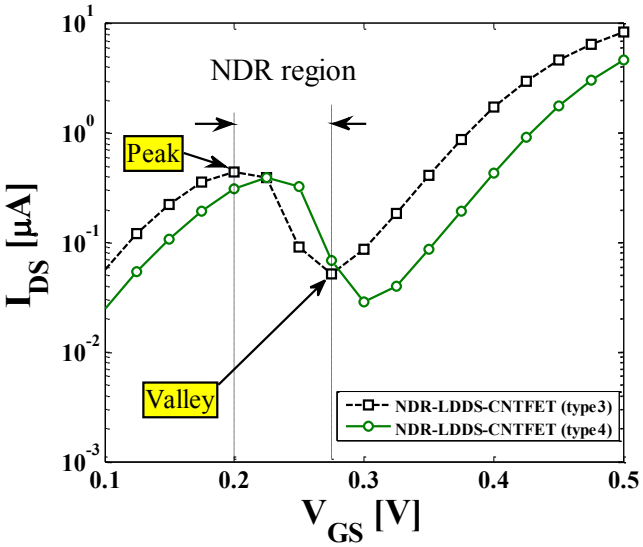

Fig. 6: The IDS-VGS characteristics of NDR-LDDS-CNTFET calculated for various types of devices of Table II at VDS=0.4 V. The NDR region has been marked for NDR-LDDS-CNTFET of type 3.

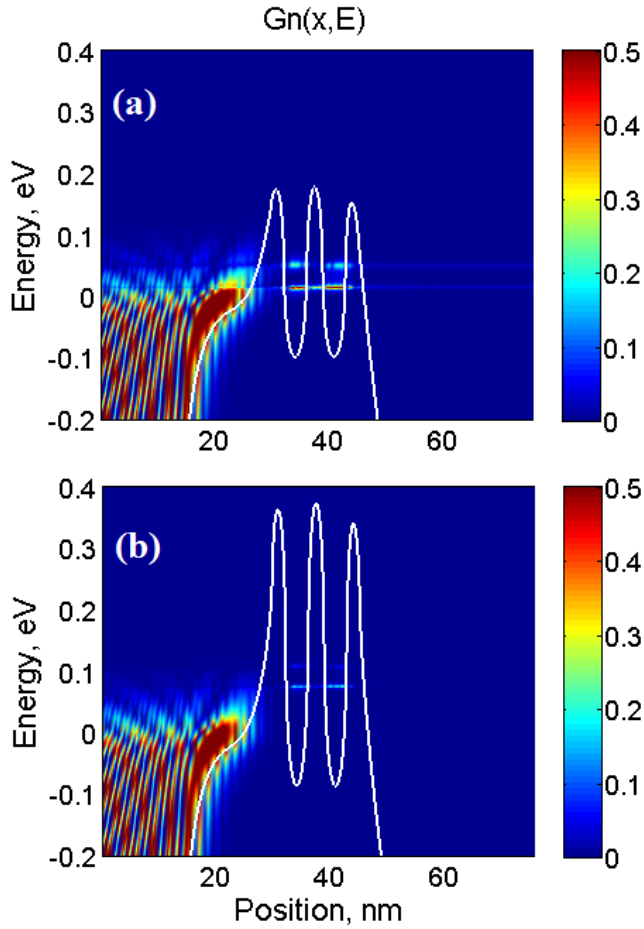

Fig. 7: The energy band diagram and color-scaled plot for the number of electrons per unit energy along the CNT axis for NDR-LDDS-CNTFET of type 2 (a) and type 3 (b) at VGS=0.1 V. The drain-source bias for the two cases is 0.4 V.

CONCLUSIONS

A nonequilibrium Green's function method has been used to simulate the proposed LDDS-CNTFET with an NDR characteristic, which is named NDR-LDDS-CNTFET. Type 1 device exhibited the NDR characteristic over the V_{GS} range of about 0.025-0.075 V. Simulations demonstrate that with the decrease in the n-type doping concentrations of regions 2 and 4, the peak and valley shifted and increased. The simulation results of type 3 structure with two n-type and three p-type regions in the channel show that the NDR characteristic over the V_{GS} range from about 0.2 to 0.275 V. It is obvious that type 3 has a larger NDR region and shifts the peak and valley of the drain-source current when compared with the type 2 structure. The effects of doping concentration on type 3 device characteristic were also investigated and discussed.

CONFLICT OF INTEREST

The authors declare that there is no conflict of interests regarding the publication of this manuscript.

REFERENCES

[1] Lee K., Lee J., Park J., and Yang K., (2015), A novel Ku-band RTD-based quadrature VCO for low power applications. *IEEE. Microwave. Wireless. Co.* 25: 328-330.

[2] Kitagawa S., Suzuki S., Asada M., (2014), 650-GHz resonant-tunneling-diode VCO with wide tuning range using varactor diode. *IEEE Elect. Dev. Let.* 35: 1215-1217.

[3] Okada K., Kasagi K., Oshima N., Suzuki S., Asada M., (2015), Resonant-tunneling-diode terahertz oscillator using patch antenna integrated on slot resonator for power radiation. *IEEE Trans. THz Sci. Technol.* 5: 613-618.

[4] Kumar A., Kumar V., Agarwal S., Basak A., Jain N., Bulusu A., Manhas S. K., (2014), Nitrogen-terminated semiconducting zigzag GNR FET with negative differential resistance. *IEEE Trans. Nanotechnol.* 13: 16-22.

[5] Kang S., Fallahazad B., Kayoung L., Movva H., (2015), Bilayer graphene-hexagonal boron nitride heterostructure negative differential resistance interlayer tunnel FETs. *IEEE Elect. Device Let.* 36: 405-407.

[6] Yu X., Mao L. H., Guo W. L., Zhang S. L., Xie S., Chen Y., (2010), Monostable–bistable transition logic element formed by tunneling real-space transfer transistors with negative differential resistance. *IEEE Elect. Dev. Let.* 31: 1224-1226.

[7] Laskar J., Bigelow J. M., Leburton J., Kolodzey J., (1992), Experimental and theoretical investigation of the DC and high-frequency characteristics of the negative differential resistance in pseudomorphic AlGaAs/InGaAs/GaAs MODFET's. *IEEE Trans. Elect. Devices.* 39: 257-263.

[8] Wu C. L. Hsu W. C., (1996), Enhanced resonant tunneling real-space transfer in δ-doped GaAshGaAs gated dual-channel transistors grown by MOCVD. *IEEE Trans. Elect. Devices.* 43: 207-212.

[9] Chen Y. W., Hsu W. C., Shieh H. M., Lin Y. S., Li Y. J., Wang T. B., (2002), High breakdown characteristic δ-doped InGaP/InGaAs/AlGaAs tunneling real-space transfer HEMT. *IEEE Trans. Elect. Devices.* 49: 221-225.

[10] Chang S., Zhao L., Lv Y., Wang H., Huang Q., He J., (2015), Negative differential resistance in graphene nanoribbon superlattice field-effect transistors. *Micro & Nano Lett.* 10: 400-403.

[11] Yousefi R., Saghafi K., Moravvej-Farshi M. K., (2010), Numerical study of lightly doped drain and source carbon nanotube field effect transistors. *IEEE Trans. Elect. Devices.* 57: 765-771.

[12] Hejazifar M. J., Sedigh Ziabari S. A., (2014), Investigation of the cutoff frequency of double linear halo lightly doped drain and source CNTFET. *Int. Nano. Lett.* 4: 118-123.

[13] Molaei Imen Abadi R., Sedigh Ziabari S. A., (2017), A Comparative Numerical Study of Junctionless and p-i-n Tunneling Carbon Nanotube Field Effect Transistor. *J. Nano Res.* 45: 55-76.

[14] Orouji A., Arefinia Z., (2009), Detailed simulation study of a dual material gate carbon nanotube field-effect transistor. *Physica. E.* 41: 552-557.

[15] Levi A. F. J., Applied Quantum Mechanics. Cambridge, Cambridge Univ. Press, 2003.